Applied Catalysis A, General 691 (2025) 120055

Contents lists available at ScienceDirect

Applied Catalysis A, General

journal homepage: www.elsevier.com/locate/apcata

Lanthanum-group elements promoted PtGa catalysts for propane dehydrogenation: Exploring key performance descriptors

Haokun Wang, Xuelei Pan, Yanjie Wang, Bryan Kit Yue Ng, Shik Chi Edman Tsang *

The Wolfson Catalysis Centre, Department of Chemistry, University of Oxford, Oxford OX1 3QR, UK

ARTICLE INFO

Keywords:
PtGa
Lanthanides
Propane dehydrogenation
Performance descriptors
Strong metal-support interactions

ABSTRACT

Propylene, a crucial component in the chemical industry, holds a prominent position as the second-largest material within petrochemicals, serving as a foundational element for major synthetic materials and essential industrial chemicals such as acetone and isopropanol. Conventional propylene production methods confront environmental challenges, promoting the investigation of alternative pathways, such as direct propane dehydrogenation. While commercial PtSn or PtGa-based catalysts have demonstrated success in propane dehydrogenation, further enhancements are imperative to mitigate operational costs. Therefore, this study utilizes four lanthanum-group elements (La, Ce, Pr, and Nd) with varying loadings (1 wt%, 3 wt%, and 5 wt%) to modify PtGa/Al_2O_3 catalyst, resulting in improved conversion, selectivity, and stability. Furthermore, this research establishes a clear structure-activity relationship based on some key performance descriptors, underscoring the effectiveness influence of reducibility, total acid concentration, and total coke content in conversion, selectivity, and stability. The impact of strong metal-support interactions on conversion and stability should also be considered, highlighting the complexities in accessing catalytic performances. The exploration of diverse performance descriptors revealed in this study contributes to the rational design of catalysts for propane dehydrogenation, addressing ongoing efforts to refine and tailor catalysts for efficient propane dehydrogenation. This study also offers valuable insights for optimizing catalytic performance across various industrial reactions, further advancing the field of catalysis and promoting sustainable and efficient chemical processes.

1. Introduction

Propylene, a pivotal constituent in the chemical industry, ranks as the second-largest starting material in petrochemicals [1]. It serves as a foundational element for the production of three major synthetic materials: plastics, synthetic rubber and synthetic fibres [2]. Moreover, propylene undergoes processing into other significant industrial chemicals, such as acetone and isopropanol [1,3,4]. Despite traditional propylene production methods, like fluid catalytic cracking (FCC) and steam cracking (SC), constituting over 80 % of industrial propylene production in 2016, they suffer from low atom-economy, involve toxic reactants, and utilize non-renewable feedstocks, and require catalyst regeneration rendering them less environmentally friendly and sustainable [4–6]. In contrast, emerging processes like direct propane dehydrogenation present a promising avenue, overcoming drawbacks associated with toxic chemicals and minimizing side-product generation under proper operation conditions [4]. Furthermore, the forecasted annual growth of propylene demand at a rate of 2–3 % by 2030 and the surge in demand during the COVID-19 pandemic for polypropylene, particularly in the production of surgical masks, underscore the need for alternative propylene production routes, including propane dehydrogenation [3,6,7].

Within the realm of propane dehydrogenation, despite its significant environmental benefits, the inherently endothermic thermodynamics mandate high operating temperatures (550 – 700 ℃) [3]. These severe conditions pose challenges to catalytic activity, selectivity and stability [8]. Therefore, the development of a catalyst that is not only active but also exhibits selectivity and stability. It is imperative for this process to be sustainable. Currently, two main types of commercial catalysts–Pt-based and CrO_x-based–are commonly available for propane dehydrogenation [6]. Beyond these, additional technologies have emerged, such as ADHO, developed by the China University of Petroleum in 2016, which utilizes refectory oxides as dehydrogenation catalysts. Similarly, in 2018, KBR's K-PRO™ technology introduced a novel catalyst system that are both non-Pt and non-Cr [6]. While CrO_x-based catalysts, owing to their low price and high catalytic activity, have been

* Corresponding author.
E-mail address: edman.tsang@chem.ox.ac.uk (S.C.E. Tsang).

https://doi.org/10.1016/j.apcata.2024.120055
Received 5 September 2024; Received in revised form 8 November 2024; Accepted 2 December 2024
Available online 5 December 2024

widely commercialized in FBD-4 and CATOFIN processes, but the high toxicity and environmental hostility push the exploration of alternative metal oxide catalysts with low or non-chromium content [6,8]. In contrast, Pt-based catalysts show an excellent ability for C-H bond activation coupled with a low tendency for C-C bonds breakage as well as an eco-friendly character. However, their high tendency to coking and sintering and high cost require the development of more selective and stable Pt-based catalysts, particularly by using appropriate promoters [4,6,9]. Among all the promoters, Sn and Ga have proven to be the most successful ones in augmenting Pt catalysts in propane dehydrogenation, as demonstrated by their application in catalysts for Oleflex ($PtSn/Al_2O_3$), Dow FCDh ($PtGa/Al_2O_3$), and other commercial processes such as STAR and PDH [10]. The use of Sn or Ga promoters leads to higher propane selectivity and increased diffusion of coke away from the active Pt sites, explained by the well-known ‘‘geometric effect’’ and ‘‘electronic effect’’ [11,12]. Despite the significant enhancement in catalytic performances using Sn or Ga promoters, the dehydrogenation capabilities of PtSn or PtGa catalysts still require further improvement to decrease the operating cost of catalysis and separation in industrial production. Therefore, various other promoters have been explored to enhance thermal stability, regulate the acid-base properties of support, and manage metal-support interactions based on PtSn or PtGa catalysts.

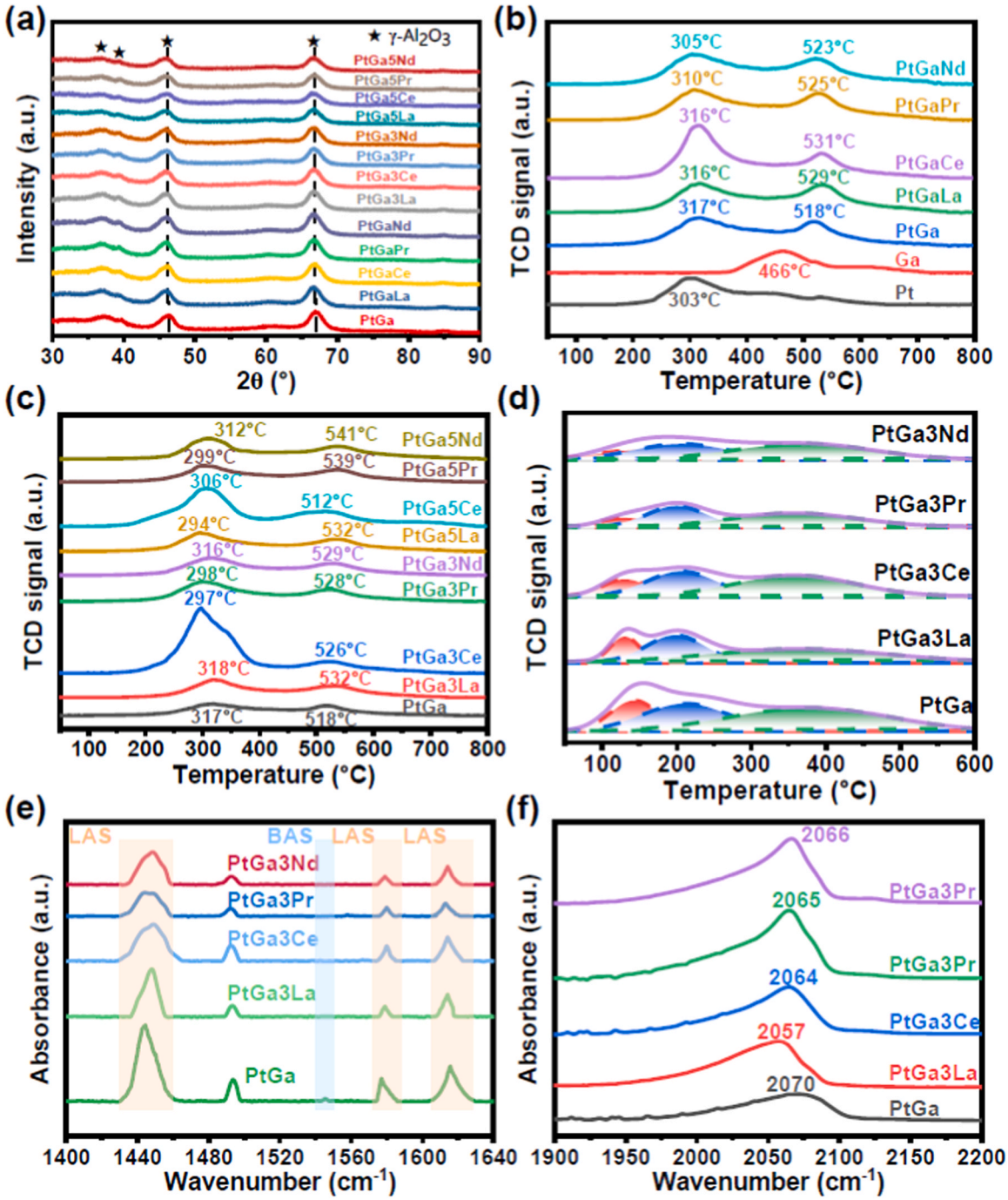

Fig. 1. (a) XRD patterns of all catalysts, (b) and (c) H_2-TPR profiles over different catalysts, (d) NH_3-TPD profiles on $PtGa/Al_2O_3$ and 3 wt% loading promoted catalysts, (e) pyridine-IR profiles on $PtGa/Al_2O_3$ and 3 wt% loading promoted catalysts at 200 ℃, and (f) CO-FTIR spectra on $PtGa/Al_2O_3$ and 3 wt% loading promoted catalysts.

These include alkaline earth metals like Mg [13], Ca [14], and numerous transition metals, such as Zn [15,16], Co [16], In [17], Fe [17], La [17–19], Ce [17,19], Y [19], and more. Among these, lanthanide promoters stand out for their superior properties. Firstly, lanthanide oxides possess a basicity comparable to that of alkali metal oxides, but without the detrimental surface poisoning effects typically associated with alkali ions. The incorporation of lanthanides helps to reduce the acidity of the catalyst support, effectively minimizing coke deposition and enhancing both catalyst stability and propylene selectivity [17]. Additionally, lanthanide elements, such as La and Ce, play a crucial role in stabilizing active sites by strengthening metal-support interactions, thereby inhibiting sintering and coke formation, which ultimately leads to improved catalytic performance [17–19]. Despite advancements in catalytic performance through the use of these lanthanide metals, the precise correlation between the diverse microenvironments of active sites modified by these promoters and their initial catalytic behaviours remains insufficiently understood. This understanding is critical for the rational design of heterogeneous catalysts. Although recent studies have begun to address this correlation in reactions like ethylene hydrogenation [20] and acetylene hydrochlorination [21], further investigation is warranted in other industrial reactions and catalysts, such as PtGa catalysts in propane dehydrogenation.

In this study, we briefly employ four lanthanum-group promotors (La, Ce, Pr, Nd) with varying metal loadings (1 wt%, 3 wt%, and 5 wt%) to modify the commercial PtGa/γ-Al_2O_3 catalyst for propane dehydrogenation. All resulting catalysts exhibit improved conversion, selectivity, and stability compared to PtGa/γ-Al_2O_3 catalyst. Furthermore, the underlying principle of these promotors allows us to carefully regulate microenvironments of active sites and facilitate exploration of key performance descriptors, constructing dependent structure-activity relationships based on PtGa/γ-Al_2O_3 catalysts for propane dehydrogenation.

2. Materials and methods

2.1. Materials

Boehmite was acquired from SCG Ltd., and a propane gas cylinder (99.5 %) was sourced from BOC Ltd. Additionally, other chemicals, including chloroplatinic acid hydrate (≥ 99.9 %), gallium (III) nitrate hydrate (99.9 %), lanthanum (III) nitrate hexahydrate (99.99 %), cerium (III) nitrate hexahydrate (99.99 %), praseodymium (III) nitrate hexahydrate (99.9 %), and neodymium (III) nitrate hexahydrate (99.9 %) were all ordered from Sigma-Aldrich. All chemicals were used as received.

2.2. Catalyst preparation

The catalyst support, γ-Al_2O_3, was synthesized by calcining boehmite at 600 ℃ for 8 h in air. PtGa/γ-Al_2O_3 catalysts (Pt: 1 wt%, Ga: 3 wt%) with varying loadings (from 0 wt% to 5 wt%) of promoters (La, Ce, Pr and Nd) were prepared using a standard co-impregnation method. The Pt and Ga loadings were selected based on optimal performance reported in literature [22]. Chloroplatinic acid hydrate, gallium (III) nitrate hydrate, lanthanum (III) nitrate hexahydrate, cerium (III) nitrate hexahydrate, praseodymium (III) nitrate hexahydrate, and neodymium (III) nitrate hexahydrate served as precursors, pre-dissolved in deionized water before impregnating the γ-Al_2O_3 support into the solution at room temperature for 5 h with stirring. Subsequently, the slurry was dried at 100 ℃ overnight, and the dried solid was calcined at 550 ℃ for 6 h in air at a heating rate 5 ℃min^{-1}.

2.3. Characterization

Detailed methods for catalyst characterization, including X-ray diffraction (XRD), Brunauer-Emmett-Teller (BET) surface area, temperature-programmed desorption of ammonia (NH_3-TPD), temperature-programmed reduction of hydrogen (H_2-TPR), thermogravimetric (TG) analysis, Raman spectra, Fourier transform infrared measurement using carbon monoxide as the probe molecular (CO-FTIR), pyridine as the probe molecular (pyridine-IR), and in-situ diffuse reflectance infrared Fourier-transform spectroscopy (DRIFTS), X-ray photoelectron spectroscopy (XPS), high-resolution transmission electron microscopy (HRTEM) are comprehensively detailed in the Supporting Information.

2.4. Catalytic tests

The propane dehydrogenation reaction was executed in a fixed-bed reactor featuring an inner diameter of 3/8 in. and a length of 15 in. In a standard experiment, 0.1 g of catalyst was loaded into the middle of reactor, with quartz wool packed at both ends. The catalyst underwent heating to 600 ℃ in 1 h and subsequent reduction in 20 mLmin^{-1} pure H_2 flow for 2 h. Two reactant gas mixtures were used: one with hydrogen, comprising 10 vol% H_2 and 20 vol% C_3H_8, balanced with N_2 at a total flow rate 25 mLmin^{-1}; and one without hydrogen, comprising 20 vol% C_3H_8, balanced with N_2 at a total flow rate 25 mLmin^{-1}. The weight hourly space velocity (WHSV) of propane was maintained at 5.4 h^{-1} under both conditions. After introducing the reactant gas into the reactor for 10 min, the gas products were analyzed using an online Shimadzu GC-2014 gas chromatography equipped with a flame ionization detector (FID). Long-term stability tests were performed under the same reaction conditions with hydrogen-free gas mixtures. After each 14-hour reaction, the catalysts were regenerated by feeding 20 mLmin^{-1} air for 1 h at 600 ℃, followed by reduction in 20 mLmin^{-1} H_2 flow for 2 h before the next cycle. Propane conversion, propylene selectivity, and carbon balance were calculated using the following expressions:

$$C_3H_8\ \text{conversion}(\%) = \frac{\left[F_{C_3H_8}\right]_{in} - \left[F_{C_3H_8}\right]_{out}}{\left[F_{C_3H_8}\right]_{in}} \times 100\ \% \quad (1)$$

$$C_3H_6\ \text{selectivity}(\%) = \frac{\left[F_{C_3H_6}\right]_{out}}{\left[F_{C_3H_6}\right]_{out} + \frac{2}{3}\left[F_{C_2H_6}\right]_{out} + \frac{2}{3}\left[F_{C_2H_4}\right]_{out} + \frac{1}{3}\left[F_{CH_4}\right]_{out}} \times 100\ \% \quad (2)$$

$$\text{Carbon balance}(\%) = \frac{\left[F_{C_3H_8}\right]_{out} + \left[F_{C_3H_6}\right]_{out} + \frac{2}{3}\left[F_{C_2H_6}\right]_{out} + \frac{2}{3}\left[F_{C_2H_4}\right]_{out} + \frac{1}{3}\left[F_{CH_4}\right]_{out}}{\left[F_{C_3H_8}\right]_{in}} \times 100\ \% \quad (3)$$

The deactivation rate constant k_d (h^{-1}) and expected catalyst life τ (h) are determined by fitting the propane conversion to the first-order deactivation model using the following equation:

$$k_d(h^{-1}) = \frac{\ln\left(\frac{1-con_{end}}{con_{end}}\right) - \ln\left(\frac{1-con_{start}}{con_{start}}\right)}{t} \quad (4)$$

$$\tau(h) = \frac{1}{k_d} \quad (5)$$

where, con_{start} and con_{end} represent the initial and final propane conversion, respectively, and t denotes the reaction time; a higher k_d value and lower τ value indicate a poorer stability [23].

3. Results and discussion

3.1. Physicochemical properties of catalysts

In Fig. 1(a), the XRD patterns of PtGa/γ-Al_2O_3 sample exhibits prominent diffraction peaks at 37.7°, 45.8°, and 66.9°, corresponding to (311), (400), and (440) planes of γ-Al_2O_3 [24]. Upon the introduction of lanthanum-group elements into the PtGa system, a discernible shift of the main diffraction peaks towards lower angles is observed in all-modified catalysts, indicative of an expansion in lattice parameters [25]. This expansion is ascribed to the larger size of the cations of these promoters compared to Al^{3+}, with some of these cations occupying the position of Al in γ-Al_2O_3 lattice, leading to the structural lattice expansion. Importantly, no diffraction peaks for Pt, Ga, and other promoters are detected, suggesting that all these elements are well-dispersed over the γ-Al_2O_3 support. This conclusion is further affirmed by the HRTEM image of PtGa/γ-Al_2O_3 catalyst in Figure S1, revealing a relatively homogeneous distribution of metallic particles with an average particle size around 1.7 nm. Further insights into the specific surface area and pore size distribution of all catalysts are obtained through nitrogen adsorption/desorption isotherms (Figure S2 and S3). Interestingly, all catalysts exhibit similar patterns of adsorption-desorption isotherms and pore size distributions. Notably, the introduction of different promoters (La, Ce, Pr, Nd) up to 5 wt% does not significantly alter the specific surface area, and pore characteristics for all catalysts (Table S1). These findings collectively underscore the typical mesoporous properties of γ-Al_2O_3 support, as evidenced by the type IV adsorption isotherms and negative t-plot micropore volume.

To evaluate the reducibility of diverse supported catalysts, H_2-TPR experiments are conducted, and the resulting profiles are depicted in Fig. 1(b) and (c). In Fig. 1(b), when Pt is exclusively supported on the γ-Al_2O_3 support, a notable reduction peak emerges around 303 ℃, indicating the facile reduction of Pt oxides to metallic Pt over Al_2O_3, typically occurring below 400℃ [22]. In contrast, the reduction of Ga oxides over the same support presents more challenging than that of Pt, as evidenced by the higher temperature of 466 ℃ (Fig. 1(b)). A similarly intense reduction peak is observed over Ga/ZSM5 catalysts between 400℃ and 600 ℃, attributed to the first stage reduction of Ga^{3+} to Ga^{+}, supported by TPR-microbalance studies and theoretical calculations [26,27]. When Pt and Ga coexist on the Al_2O_3 support, two typical prominent reduction peaks are observed at 317℃ and 518℃, respectively. Wang et al. (2016) noted two similar reduction peaks over PtGa/Al_2O_3 but at lower temperatures (239℃ and 440℃), possibly due to variations in Ga content, leading to distinct TPR profiles for bimetallic catalysts [22], [28]. Notably, the lower peak within the temperature range of Pt oxides reduction requires a slightly higher temperature (317℃) than Pt alone (303℃). This suggests the simultaneous reduction of Pt and a fraction of Ga in intimate contact, forming intermetallic PtGa species [29]. The higher temperature reduction peak may result from the reduction of a fraction of remote Ga physically separated from Pt, but catalyzed by Pt [28]. It has been reported that Pt presence can promote the reduction of remote Ga oxides, even when located on separate grains [30–32]. According to this theory, H_2 would be dissociate on metallic Pt sites, and the resulting atomic hydrogen would be responsible for the Ga reduction at this elevated temperature. Overall, the two reduction peaks signify two distinct types of Ga species physically located on the surface from Pt: one in intimate contact with Pt and the other localized on the support [28].

The introduction of diverse promoters (La, Ce, Pr, Nd) at low loading (1 wt%) in Fig. 1(b) induces a progressive shift in the first peak temperatures to lower values (compared to PtGa) accordingly, while the second peaks shift to higher values. The lower temperatures of the first peaks, guided by their intrinsic nature, suggest that these promoters contribute to facilitate the reduction of the intimate-contact Pt with a fraction of Ga species, thereby facilitating the formation of PtGa species. The increase in surface coverage of promotors could also reduce the Pt-assisted reduction of remote Ga species hence raising the second reduction temperature. Vu et al. (2011) observed a similar facilitation of Pt species reduction with the addition of La and Ce to Pt/Al_2O_3 [19]. This decrease in the first reduction peak is attributed to the electron-pushing effect, wherein the increasing density conglomeration of electron charge on the Pt surface, promotes electron transfer from Ga to Pt. This phenomenon is observed in La-modified PtSn systems as well, which is thought to be related to Lewis basicity of the ionic lanthanide oxides as promotors [32]. In contrast to La, Pr, and Nd, Ce-promoted PtGa catalyst not only attenuates the 1st reduction temperature but also nearly doubles this reduction peak area with broader peak ranges, indicative of a unique interaction between Pt, Ga, and Ce over the support. Our recent work also identified comparable strong interactions between Pt, Sn and Ce over amorphous SiAl support [33]. The decreased reduction temperature over Ce-promoted catalyst not only suggests a strong Lewis base interaction with PtGa but also a distinctive metal-support interaction phenomenon, likely due to enhanced hydrogen spillover from Pt to more remote Ga species via surface cerium oxides. Additionally, the preferential interaction of Pt with ceria compared to that with alumina may further reinforce this effect [34]. As a result, the hydrogen consumption over the first reduction peak, at the expense of second peak area, dramatically increases compared to the non-promoted condition, indicating a greater degree of PtGa alloy reduction and potentially enhancing catalytic performances with Ce as a promoter. Unlike other promoters (La, Pr, and Nd), Ce oxides are also partially reducible, which could contribute to the increased hydrogen consumption in the first reduction peak. To access this possibility, we conducted H_2-TPR experiments on Pt5Ce/Al_2O_3 and compare the results with current H_2-TPR profiles. As illustrated in Figure S4, the Pt5Ce/Al_2O_3 sample indeed shows slightly elevated hydrogen consumption within the 250–350 °C range compared to Pt/Al_2O_3 alone, suggesting only a partial reduction of cerium oxides even at 5 wt% Ce loading. However, the increase observed in Ce-modified PtGa-based samples is notably higher. These results strongly indicate that while cerium oxide reduction may contribute to marginally to hydrogen consumption within this temperature range, the significant increase in Ce-modified PtGa samples primarily arises from the strong interactions among Pt, Ga, and Ce on the Al_2O_3 support, rather than cerium oxide reduction alone.

Upon the further introduction of these promoters at 3 wt% and 5 wt % in Fig. 1(c), the temperature shifts of the first peak temperatures become more pronounced, suggesting a promotion of the reduction of intimate-contact Pt and Ga. This affirms that both the types and loadings of promoters are responsible for their reducible behaviors [19,35]. Similar to Ce's strong interactions between Pt, Ga, and Ce at low promoters loading (1 wt%), these interactions are reinforced at middle (3 wt%) and high loadings (5 wt%), as evidenced by higher peak area and broader peak ranges. Despite the broadest peak occurring at 5 wt% Ce loading, indicative of the strongest interactions, the largest peak area is observed over 3 wt% Ce loading. Interestingly, the introduction of Ce loading from 3 wt% to 5 wt% shifts the first peak temperature to a higher value, while the second one shifts to a lower value. This suggests that excessive deposition of Ce impairs the intimate-contact Pt (a high affinity of Pt coverage with Ce) and Ga but does not affect much on the reduction of the remote Ga species. In contrast, the electron-pushing

Table 1
Summary of acidity results from NH_3-TPD and pyridine-IR at 200 ℃.

Catalyst	T_M (℃)			Total area (a.u.)	Peak fraction (%)			LAS concentration from pyridine-IR (μmol g cat^{-1})
	I	II	III		I	II	III	
PtGa	143	212	379	28	19	32	49	57.6
PtGaLa	132	207	371	20	13	39	48	43.7
PtGaCe	132	204	361	20	14	38	48	43.4
PtGaPr	138	210	368	21	14	39	47	44.8
PtGaNd	141	207	375	24	13	37	50	52.7
PtGa3La	130	198	365	16	16	35	49	33.0
PtGa3Ce	130	206	359	18	15	35	50	40.9
PtGa3Pr	129	200	358	12	12	37	51	26.8
PtGa3Nd	139	206	370	16	15	35	50	33.2
PtGa5La	135	201	370	14	14	34	52	30.4
PtGa5Ce	131	202	355	14	14	36	50	30.1
PtGa5Pr	132	202	363	16	16	34	50	33.8
PtGa5Nd	140	212	372	18	15	36	49	38.1

effects originating from other promoters (La, Pr, and Nd) are strengthened with further increase in these promoters' loadings, confirmed by higher hydrogen consumption of the first peaks at 5 wt% than that at 3 wt%.

NH_3-TPD is employed to meticulously examine the concentration and strength of various acids sites, as illustrated in Fig. 1(d), Figure S5 and S6. Semiquantitative deconvolving of the resulting NH_3-TPD profiles is conducted, and the fitting results are summarized in Table 1. Within the temperature range of 50℃ to 600℃, all catalysts exhibit three distinct peaks, categorized as weak acid sites (red dashed lines), medium acid sites (blue dashed lines), and strong acid sites (green dashed lines) based on their desorption strengths. Upon introducing different promoters, a discernible trend emerges: all promoted catalysts showcase a decrease in the total concentration of acid sites and weakening the strength for all three acid sites. This is corroborated by the reduced total peak area and decreased desorption temperatures outlined in Table 1. Intriguingly, the progressive introduction of promoters consistently diminishes the strength and concentration of acid sites, while each peak fraction remains unaltered. This implies that the impact of these promoters is associated with the overall acidity rather than targeting a specific acid site.

Due to the limitations of NH_3-TPD in clarifying the nature of acid sites, pyridine-IR analysis was conducted at 200 ℃ to evaluate the total concentration of Brønsted acid sites (BAS) and Lewis acid sites (LAS). As shown in Fig. 1(e), the peaks around 1450 cm^{-1} correspond to LAS interactions with pyridine, while BAS is nearly undetectable (peaks around 1550 cm^{-1}), indicating that the acidity of all catalysts originates from LAS. Furthermore, LAS concentration was calculated using Beer-Lambert-Bouguer law [36], with results summarized in Table 1. The trends in LAS concentration from pyridine-IR align with NH_3-TPD findings, showing a gradual decrease in LAS concentration with the introduction of promoters. Similar reductions in acidity concentration were observed with the gradual increase in La content over ZSM-5 zeolite [37]. These reductions can be elucidated by the obstruction of the ZSM5 pore entrance due to La_2O_3 deposition and the creation of new basic sites on the support surface. However, in our study, the introduction of various promoters up to 5 wt% does not notably affect the specific surface area and pore distribution, as evidenced by adsorption/desorption isotherms and pore size distribution in Figure S2 and S3. Thus, the sole reason behind this phenomenon is the generation of new basic sites.

Previous studies have shown that the introduction of La can significantly enhance the basicity of the ZSM5 support, as assessed by CO_2-TPD [38,39]. A new peak around 70 ℃ was observed, reflecting the presence of surface basic sites with the introduction of La promoters. Furthermore, the amount of CO_2 adsorbed calculated over the peak at 70 ℃, increased with the amount of La loading increase, indicating that the newly generated basic sites on the surface result from the introduction of La promoters. As discussed, the bonds in the lattice of lanthanide oxides are mainly ionic, which is a result of the elements' electronegativity. The typical properties of lanthanide oxides are basic oxides, and their basicity is known to be comparable to that of alkali metal oxides but avoiding the surface poisoning by alkali ions. These newly formed basic sites could impede the re-adsorption of the generated propylene and suppress deep cracking, leading to higher propylene selectivity. Similarly, the decreased concentration and strength of acid sites also confer advantages for the overall catalytic performances. This is attributed to the inhabitation of the side reactions, such as isomerization and polymerization, which are typically catalyzed by these acid centers, ultimately preventing coke deposition [40].

The investigation of Pt interaction with various promoters extends to the alternations of the electronic environment of Pt atoms, employed CO as probe molecule for Fourier transform infrared (CO-FTIR) spectra characterization, as depicted in Fig. 1(f). All tested catalysts showcase a primary peak centered between 2057 cm^{-1} to 2070 cm^{-1}, indicative of CO linearly bonded to a surface-exposed metallic Pt atom [41]. The introduction of an appropriate amount of promoters could induce a red shift in adsorption, moving from 2070 cm^{-1} over PtGa catalyst to the lowest frequency of 2057 cm^{-1} over PtGa3La catalyst. This shift signifies CO coordinated with Pt atoms, within the electrons of surface Pt occupy 2π antibonding orbital of CO molecules, resulting in Pt-C bond formation and weakening of C-O bond energy. Moreover, the addition of these basic promoters augments the electron density of Pt particles, further reducing the C-O bond energy and causing the red-shift in CO adsorption. According to Blyholder's classic model regarding the bonding of CO molecules to metal surfaces [42], the average bonding number of each Pt in smaller Pt particles is lower than that in larger particles. Therefore, the lower bonding energy may also contribute to the improved Pt dispersion facilitated by the introduction of these promoters. Of particular interest is the observed frequency increase from 2057 cm^{-1} over the La promoter to 2066 cm^{-1} over the Nd promoter. This gradual transition may stem from the progressive rise in electronegativity from La to Nd, consequently diminishing the ability to increase the electron density of Pt particles.

3.2. Catalytic performances over propane dehydrogenation

Fig. 2 presents propane conversion and propylene selectivity as functions of time on stream (TOS) over various modified catalysts at 600℃ under different reaction conditions. Using the first-order deactivation model, we calculated the deactivation rate and expected catalyst life for each catalyst under different reaction conditions, with results summarized in Table S2. As shown in Fig. 2(a)-(d), catalysts promoted by La, Ce, Pr, and Nd consistently demonstrate superior conversion, selectivity, and stability compared to the commercial PtGa catalyst under hydrogen cofeeding conditions. Notably, the PtGa3Nd catalyst achieves an initial conversion of 43.6 %, significantly higher than the unmodified PtGa catalyst (30.1 %). Interestingly, optimal conversion for each promoter is typically observed at a moderate loading (3 %) of the promoter, expect for Ce promoter, where the highest conversion is associated with high Ce loading (5 wt%). This phenomenon may be attributed to the gradually strengthened interaction between Pt, Ga, and Ce as Ce loading increases, an effect less pronounced with other promoters.

In terms of propylene selectivity, PtGa3Pr exhibits the highest selectivity, exceeding 98 %, approximately 10 % higher than the commercial PtGa catalyst. While PtGa3Pr demonstrates the best selectivity, the modified catalysts show limited variation in selectivity across different loadings or promoters. However, stability is significantly influenced by the type and loading of promoters. According to Table S2, PtGa3Ce emerges as the most stable catalyst, exhibiting a deactivation rate of approximately 0.011 h^{-1}, a 74 % reduction compared to the commercial PtGa catalyst (0.042 h^{-1}) under hydrogen cofeeding

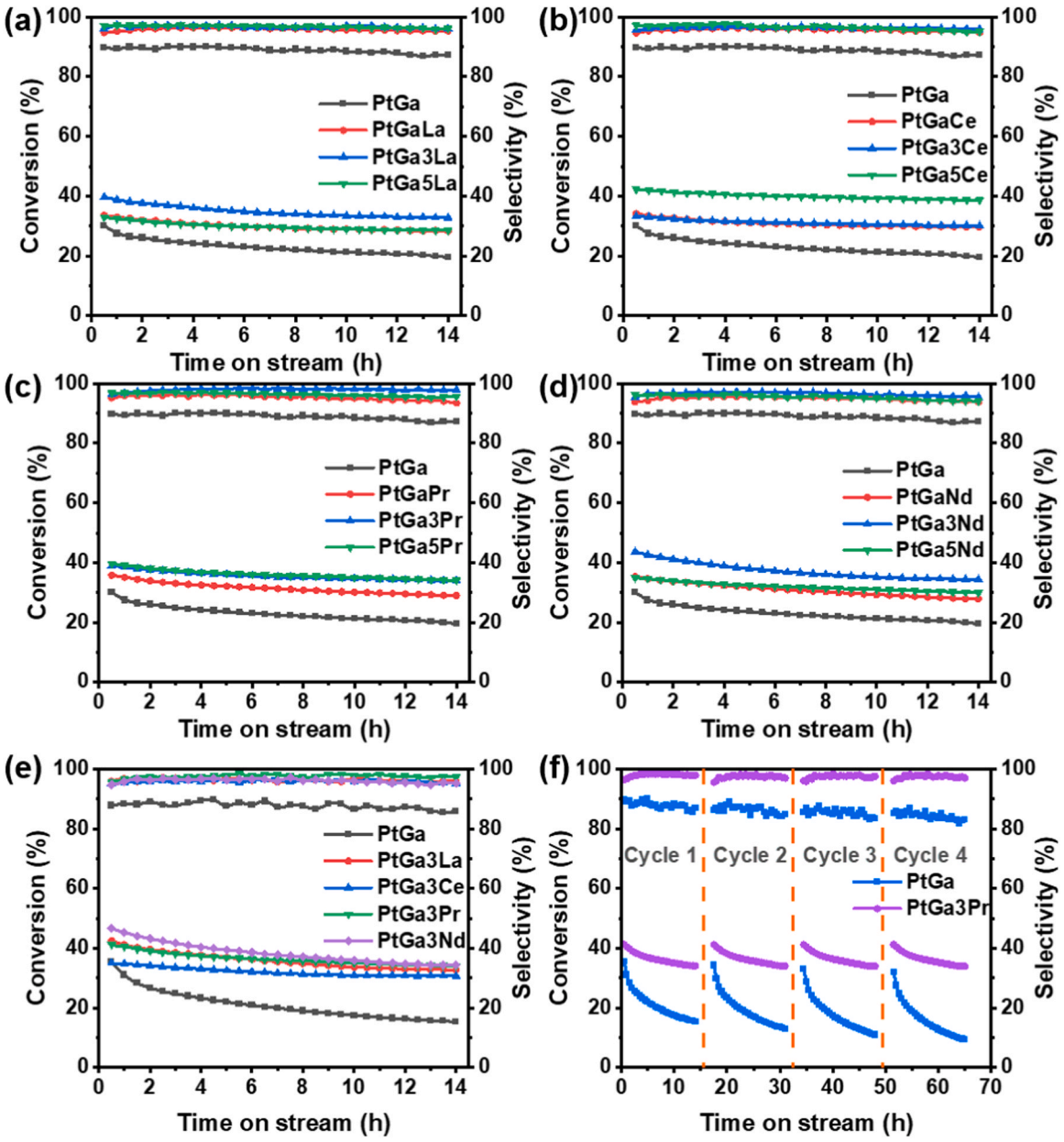

Fig. 2. Catalytic performances of modified PtGa/Al_2O_3 catalysts with various lanthanum-group promoters under different conditions: (a)-(d) La-, Ce-, Pr-, and Nd-modified catalysts under hydrogen cofeeding with varied promoter loadings, (e) La-, Ce-, Pr-, and Nd-modified catalysts under hydrogen-free conditions, and (f) PtGa and PtGa3Pr catalysts under hydrogen-free conditions across four reaction-regeneration cycles. Reaction conditions for (a)-(d): 600 ℃, total flow rate of 25 mL min^{-1} containing 10 vol% H_2, 20 vol% C_3H_8, balanced with N_2. For (e) and (f): 600 ℃, total flow rate 25 mL min^{-1} containing 20 vol% C_3H_8, balanced with N_2. The WHSV of propane was maintained at 5.4 h^{-1} for all conditions, with carbon balance exceeding 98 %.

conditions. Furthermore, compared to low loading of promoters, the deactivation rate tends to decrease with gradual loading increases. Notably, Ce-modified catalysts consistently exhibit better stability than other promoters at equivalent loadings, suggesting a correlation between strong interactions and catalyst stability.

Although hydrogen cofeeding can effectively decrease the rate of coke formation and increase catalyst stability, it restricts the conversion equilibrium [43,44]. Therefore, harsher reaction conditions without hydrogen cofeeding were tested to meet industrial production requirements. As shown in Fig. 2(e), the same propane flow rate (WHSV = 5.4 h^{-1}) without hydrogen was used to reevaluate the catalyst performances. The initial conversion of propane increased slightly compared to hydrogen cofeeding conditions across all evaluated catalysts, indicating a restriction of reaction equilibrium under hydrogen conditions. However, the stability of all catalysts was worse without hydrogen. The PtGa/Al_2O_3 catalyst exhibited nearly double the deactivation rate compared to hydrogen conditions (see Table S2), while all modified catalysts showed around a 30–40 % increase, demonstrating better coking-resistance than the nonmodified PtGa/Al_2O_3 catalyst. Despite the introduction of different promoters significantly improving the stability compared to the PtGa catalyst, deactivation still occurred over time without hydrogen. It is widely acknowledged that coke deposition and gradual deactivation over Pt-based catalysts in propane dehydrogenation are inevitable, making periodic catalyst regeneration necessary in industry to achieve sufficient total catalyst lifetime [45,46]. Therefore, further long-term stability tests were conducted with frequent regeneration cycles after 14-hours reaction periods, as illustrated in Fig. 2(f). PtGa/Al_2O_3 exhibited significant losses in activity and selectivity after regeneration cycles. In contrast, the PtGa3Pr/Al_2O_3 catalyst maintained activity and selectivity over four consecutive cycles,

confirming its better stability during regeneration. The increased stability could effectively prolong the overall catalyst lifetime and reduce the frequency of regeneration, thereby offering valuable slights for industry application.

In our PtGa-based catalysts, the role of Ga as an active site in propane dehydrogenation has been investigated, primarily due to its capacity to create LAS that facilitate hydrocarbon dehydrogenation [4,6,47,48]. Ga sites, generally present in the Ga^{3+} oxidation state, exhibit significant Lewis acidity, which also activates C–H bonds in propane, thus promoting the formation of propylene and hydrogen. Accordingly, Ga-based catalysts have also been employed as active components capable of catalyzing dehydrogenation even in the absence of Pt. However, Ga-based catalysts often face notable limitations, such as reduced stability and increased susceptibility to deactivation from coke deposition and the sintering of GaO_x species under elevated dehydrogenation temperatures [4]. Furthermore, Ga-based catalysts demonstrated considerably lower activity than Pt-based catalysts, validated by our supplementary experiments performed under identical reaction conditions with hydrogen cofeeding. As shown in Figure S7, our tests reveal that although the pure Ga/Al_2O_3 catalyst can catalyze propane dehydrogenation, its conversion is roughly an order of magnitude lower, and its propylene selectivity is over 10 % lower than that of Pt-based systems. These findings indicate that, within PtGa-based catalysts, Ga primarily serves as a promoter, inducing well-established ‘‘electronic and geometrical effects’’ that enhance the activity of Pt in propane dehydrogenation, rather than acting as a primary active site.

With regard to the active structures in PtGa-based catalysts, the formation of PtGa alloys results from the strong Pt-Ga interaction under high-temperature synthesis conditions, which drives alloy formation. Literature reports indicate that, during reduction at elevated temperatures (e.g., 500 °C), Ga^{3+} undergo partially reduced to Ga^0, a process facilitated by Pt serving as an active reduction site. The reduced Ga atoms subsequently incorporate into the Pt lattice, leading to the formation of the PtGa intermetallic phase [22,49]. Upon introducing lanthanide elements such as La, Ce, Pr, and Nd as promoters, these elements do not form intermetallic alloys with Pt; instead, their primarily modulate the catalyst’s electronic and structural properties through indirect interactions, as confirmed by H_2-TPR and CO-FTIR in Fig. 1(c) and (f). Thus, the active structure in our lanthanide-promoted PtGa--based catalysts is proposed as a stabilized PtGa alloy, further enhanced by the influence of lanthanide oxides.

3.3. *Exploring the key catalytic performance descriptors*

In the pursuit of enhancing the catalytic performance of the PtGa catalyst for propane dehydrogenation, various promoters (La, Ce, Pr, and Nd) at different loadings (1 wt%, 3 wt%, and 5 wt%) have been systematically employed. However, the discernible correlations between microenvironmental alterations over active sites and the resultant catalytic enhancements remain elusive. Consequently, this section aims to elucidate the key performance descriptors under these modified commercial catalysts for this industrially significant reaction (see Fig. 3(a)).

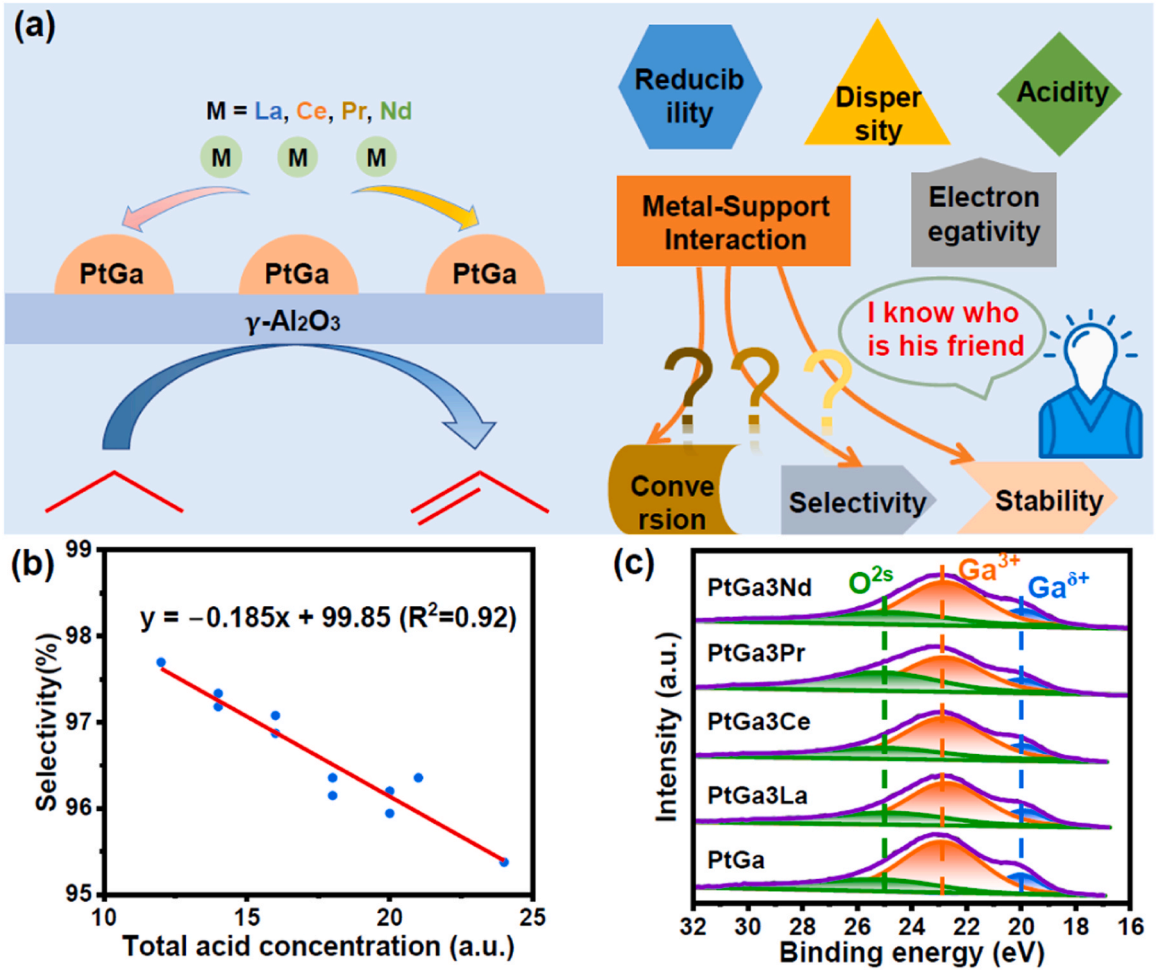

Fig. 3. (a) the schematic objective of this research paper, (b) linear fitting of total acid concentration from NH_3-TPD and propylene selectivity, and (c) XPS spectra of Ga 3d over different PtGa catalysts.

3.3.1. Exploring the key propane conversion descriptors

It is well-established that Pt nanoparticles serve as the active centres for propane dehydrogenation, with the decorating effect of second Sn/Ga promoter playing a determinative role in overall activity [22,50]. Thus, changes in the microenvironment over the generated PtGa alloy can be effectively employed as key descriptors of conversion. As observed in Fig. 2, the introduction of low loading (1 wt%) of promoters significantly enhances the reducibility of intimate-contact PtGa species compared to the commercial PtGa catalyst, evident in the increased hydrogen consumption (peak area) for the first reduction peak in H_2-TPR (see Fig. 1(b)). In the case of La, Pr, and Nd promoters, this enhancement is attributed to the electron-pushing effect, where the increasing density conglomeration of electron charge on the Pt surface promotes electron transfer from Ga to Pt [51]. Upon further introduction of these promoters (3 wt%), the push-effect is further strengthened, as evidenced by the lower temperature or especially the increased hydrogen consumption for the first reduction peak compared to low loading conditions. Consequently, the improved reducibility of PtGa species leads to better propane conversion than at lower loadings, as shown in Fig. 2. While lanthanide elements contain partially filled f-orbitals, these orbitals are typically localized and play a minimal role in direct bonding interactions, unlike the more delocalized d-orbitals commonly found in transition metals. In catalysis, the promotional effects of lanthanides are typically attributed to modulate the electronic environment of the active metal sites, such as Pt, through indirect interactions rather than through direct involvement of f-electrons. As such, although f-orbitals are present, their direct contributions in this catalytic system are minimal.

However, the introduction of high loading (5 wt%) of promoters, while further enhancing the reduction of PtGa species, dose not translate directly into improved conversion. This is attributed to the increasing challenges in reducing other localized Ga species at high promoter loadings. As indicated in Fig. 1(b) and (c), when La, Pr, and Nd loadings are increased from 1 wt% to 3 wt%, the reducibility of other localized Ga spices remains largely unchanged, judging from the similar temperatures and hydrogen consumption for the second reduction peak in TPR. Yet, with further introduction of promoters, especially at 5 wt% Pr and Nd, temperatures of these peaks dramatically increase, reaching around 540 ℃. Considering the formation of PtGa alloy, literature suggests a stepwise process: the fast formation of Pt clusters at low temperatures from readily reducible isolated Pt oxides, followed by the reaction of Pt nanoparticles with isolated Ga^{3+} sites to generate alloyed PtGa particles [8,52]. Hence, difficulties in reducing Ga^{3+} by the presence of large quantity of promotors as physical barrier inhibit the formation of PtGa species, leading to lower overall propane dehydrogenation conversion. The even lower temperatures for the first peak at high loading could be attributed to a lower amount of Ga species participating in the formation of PtGa species.

Despite of the effectiveness of reducibility as a conversion descriptor for La, Pr, and Nd promoters, Ce-modified catalysts exhibit distinct behaviors due to strong metal-support interactions. The reduction patterns of Ce-modified catalysts differ from those of the other three promoters, as depicted in Fig. 1(b) and (c). As Ce loading gradually increases up to 5 wt%, both reduction peaks widen, suggesting stronger interactions between Pt, Ga, and Ce elements over the support. This continued strengthening of interactions may be associated with higher dispersion, ultimately leading to higher propane conversion. In summary, while the reducibility proves to be an effective conversion descriptor in this reaction, the influence of metal-support interactions should not be overlooked, especially in the case of Ce-modified catalysts.

3.3.2. Exploring the key propylene selectivity descriptors

In the exploration of key propylene selectivity descriptors for propane dehydrogenation, we recognize the impact of major side reactions – cracking, hydrogenolysis, olefin isomerization, and olefin polymerization [35,40]. As these reactions predominantly unfold over acid sites, our aim is to establish connections between total acid sites and propylene selectivity. Remarkably, by correlating total acid concentration derived from NH_3-TPD profiles across various modified catalysts with their propylene selectivity under hydrogen conditions, a robust linear relationship emerges (Fig. 3(b)). This finding suggests that total acid concentration serves as a key effective propylene selectivity descriptor, wherein reduced acid concentration enhances propylene selectivity by inhibiting side reactions occurring over acid centers. A similar observation was made by Mitran et al. (2009), who identified a direct relationship between surface basicity from CO_2-TPD results and propylene selectivity at both 500 ℃ and 550 ℃ [53]. The electron-donating character of propylene, facilitating easier desorption from a less acidic surface, likely explains this phenomenon and prevents further reactions of propylene into other spices (as demonstrated later over in-situ diffuse reflectance infrared Fourier-transform spectroscopy).

Despite of the effectiveness of total acid concentration in predicting propylene selectivity, the well-known 'geometric effect' of the Sn/Ga promoter can also partially obscure surface Pt species, resulting in the generation of smaller Pt ensembles that minimize other side-reactions [11,50,54]. Consequently, we delve into the surface chemical properties of Ga via XPS to explore the relationship between Ga and propylene selectivity (Fig. 3(c)). The semi-quantitative fitting results of XPS spectra are summarized in Table S3. In Ga 3d spectra, an asymmetry peak attributed to reduced $Ga^{\delta+}$ species ($\delta < 2$) emerges at around 20.0 ev [3,55]. The higher binding energy at around 25.0 eV is assigned to O^{2-} 2 s peak, while the binding energy around 22.8 eV is attributed to the Ga^{3+} species [3,56]. Although the binding energy of Ga does not exhibit a significant shift with the introduction of these promoters, the ratio of each Ga compound undergoes a substantial change. With the exception of PtGa3Ce/Al_2O_3 of highest Ga content, all other modified catalysts exhibit a decreased ratio of Ga^{3+} to reduced $Ga^{\delta+}$ with the Pr-promoted catalyst showing the lowest ratio of Ga^{3+} at around 52 % (see Table S3). This phenomenon may be attributed to the strong interactions between Pt, Ga, and Ce, influencing the extensive reduction of Ga^{3+} species. As a result, the consistently decreased Ga^{3+} content over other promoted catalysts aligns with the conclusion drawn from H_2-TPR, indicating that the introduction of these promoters facilitates the deeper reduction of Ga species. More importantly, the lowest Ga^{3+} content over Pr-modified catalyst, with the lowest $Ga^{3+}/Ga^{\delta+}$ ratio, indicates that more Ga species are reduced, assisting in decorating the Pt species to give stronger ensemble effect to give small Pt and illustrating its superior selectivity compared to other promoters. In summary, while total acid concentration effectively predicts propylene selectivity, the surface chemical properties of Ga can also characterize its trend.

3.3.3. Exploring the key stability descriptors

In the assessment of key stability descriptors, coke accumulation is widely recognized as the primary factor contributing to catalyst deactivation in propane dehydrogenation, particularly for Pt-based catalysts [22,57,58]. During propane dehydrogenation, side reactions such as deep dehydrogenation, hydrogenolysis, and polymerization promote carbon deposition on active sites, forming a carbonaceous layer that progressively obstructs access to these sites. This blockage reduces the catalyst's surface area and overall activity. Furthermore, the strong adsorption of hydrocarbon species, combined with slow desorption rates, accelerates coke build-up, further diminishing catalytic performance. To quantify the coke content as an indicator, TG analysis is conducted on all spent catalysts after a 14-hours reaction under hydrogen conditions, as illustrated in Fig. 4(a). The TG profiles reveal three distinct regimes. In regime I (room temperature to 200℃), weight losses are observed across all spent catalysts, with minimal differences in loss amounts, indicative of similar amount of moisture and surface-adsorbed materials. Regime II (200℃ to 350℃) sees almost stable weight for all catalysts with only a slight change attributed to surface dihydroxylation of the support. Importantly, regime III (350℃ to 700℃) witnesses significant weight losses, varying among catalysts,

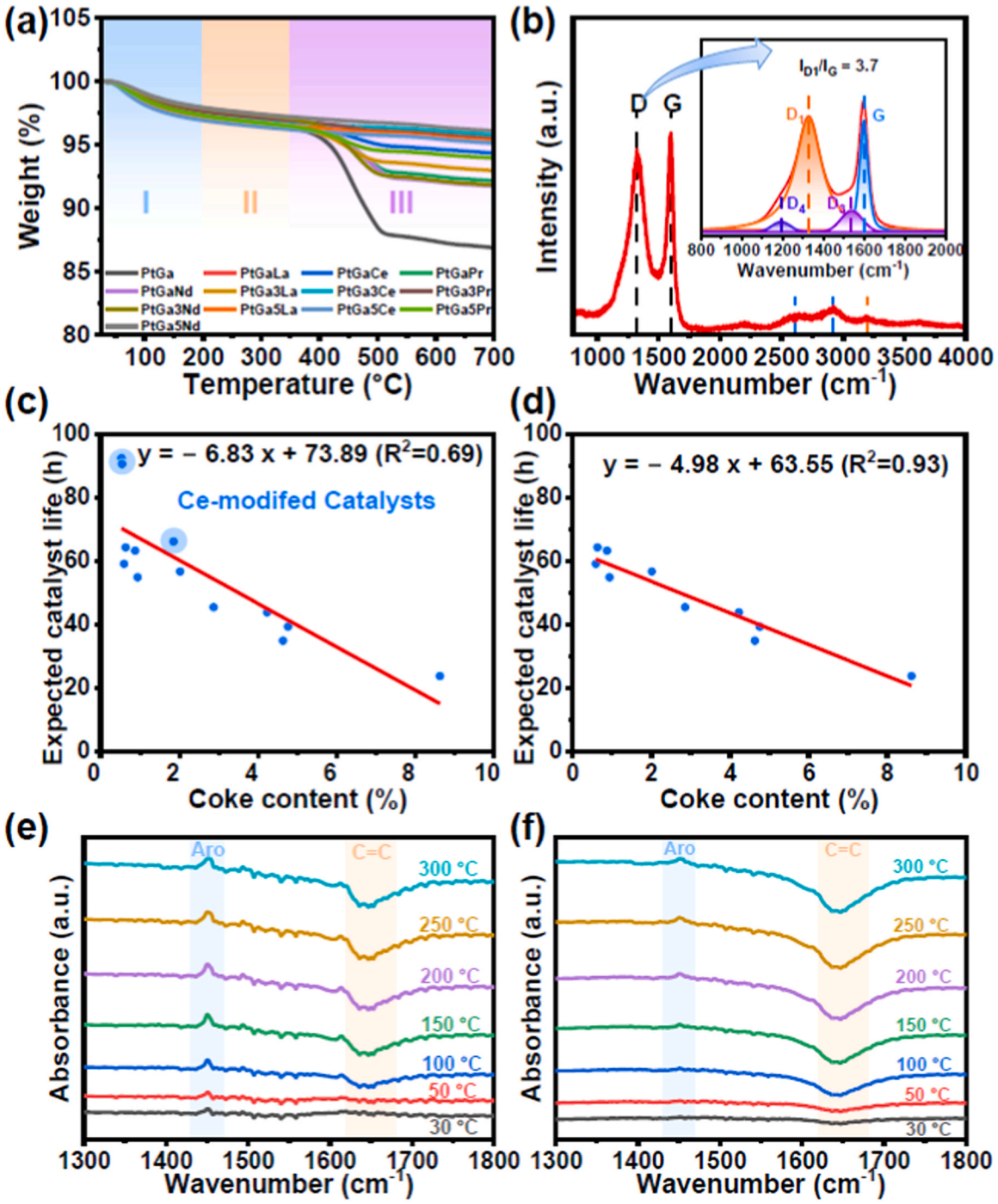

Fig. 4. (a) TG analysis results over all spent catalysts, (b) Raman spectra over spent PtGa/Al_2O_3 catalyst, (c) linear fitting of coke content against the expected catalyst life over all catalysts, (d) linear fitting of coke content against the expected catalyst life over all catalysts excluding Ce-modified catalysts, and DRIFTS of C_3H_6 adsorption over (e) PtGa/Al_2O_3 catalyst, and (f) PtGa3Pr/Al_2O_3 catalyst at different temperatures.

with PtGa/Al_2O_3 displaying the highest losses at approximately 9.5 %, while PtGa3Ce/Al_2O_3 exhibits the lowest at around 1.0 wt% (summarized in Table 2). The introduction of promoters effectively reduces coke accumulation, with increasing loading further diminishing coke content. This reduction is partially attributed to the decreased acid concentration upon gradual introduction, inhibiting the side-reaction-induced cracking leading to coke formation [59]. Simultaneously, promoter introduction facilitates propylene desorption, inhibiting deep dehydrogenation and coke formation, as demonstrated later in DRIFTS.

To elucidate the nature of the coke, Raman spectra of all spent catalysts are collected (see Fig. 4(b)). The Raman spectrum of spent PtGa/Al_2O_3 catalyst exhibits 5 identical peaks located at 1320, 1600, 2604, 2921, 3199 cm^{-1}, respectively. Peaks between 2600 and 3000 cm^{-1} (highlighted with blue dashed lines) are attributed to the vibration of C-H bonds in aliphatic hydrocarbon (robust coke), while the peak at 3199 cm^{-1} (highlighted with an orange dashed line) represents the vibration of C-H bonds in aromatics (graphitic coke) [60,61]. Therefore, the Raman spectrum suggests that the presence of both aliphatic and aromatic hydrocarbons in the coke. The Raman peaks between 1200 and 1650 cm^{-1} are further deconvoluted to analyze the detailed coke composition, as carbonaceous material Raman spectra overlap in this range [62]. The deconvolution results over PtGa/Al_2O_3 and other

Table 2
Summary of coke content from TG analysis and Raman fitting results over all spent catalysts.

Catalyst	Coke content (%)	Raman band position (cm^{-1})		
		D_1	G	I_G/I_{D1}
PtGa	9.5	1327.1	1598.4	3.7
PtGaLa	1.4	1324.6	1600.4	2.9
PtGaCe	2.3	1329	1601.1	3.1
PtGaPr	4.8	1325.9	1599.1	1.9
PtGaNd	5.3	1329.2	1600.3	2.7
PtGa3La	3.4	1324.3	1599.4	2.8
PtGa3Ce	1.0	1326.2	1598.4	3.5
PtGa3Pr	1.4	1328.2	1601	3.3
PtGa3Nd	5.2	1327.1	1600.7	3.5
PtGa5La	1.2	1326.3	1598.9	3.5
PtGa5Ce	1.1	1330.9	1599.3	4.4
PtGa5Pr	2.5	1331.2	1596.2	3.9
PtGa5Nd	1.1	1330.3	1597.9	3.9

modified catalysts are shown in Fig. 4(b) and Figure S8-S10, respectively, and the fitting results are summarized in Table 2. Four deconvoluted bands are labelled as D_4, D_1, D_3, and G bands, following literature nomenclature [63]. The G band at around 1580 cm^{-1} is attributed to an ideal graphitic lattice vibration with E_{2g} symmetry, while the D_1 band at around 1350 cm^{-1} is the defect band assigned to in-plane defects and heteroatoms (robust coke) [64,65]. In contrast, the D_3 Raman band can be attributed to amorphous carbon, and D_4 corresponds to the highly disordered graphitic lattice [66]. In Fig. 4(b), the G band is located at 1598.4 cm^{-1}, which is higher than that of a perfect large graphite crystal (1575 cm^{-1}), suggesting that this coke could be graphite-like carbon species. With the introduction of promoters, the G band shifts to higher wavenumbers, suggesting a smaller crystal size of this coke compared to that over $PtGa/Al_2O_3$ catalyst [67]. More importantly, the introduction of promoters can also subtly reduce the ratio of I_G/I_{D1}, indicating a lower graphitization degree of coke, particularly for the low and moderate loadings [68].

Considering the diverse nature of coke types, the removal of coke particularly graphitic coke typically necessitates higher temperatures, attributing the weight loss in regime III of TG analysis to coke [69]. Establishing a relationship between coke content and the expected catalyst life across different catalysts is essential, as depicted in Fig. 4(c). A robust linear correlation is achieved by fitting coke content against expected catalyst life, although it's notable that Ce-modified catalysts deviate the fitting line, exhibiting a longer expected life at similar coke content compared to other promoted catalysts. This deviation is attributed to the unique strong and peculiar metal-support interactions over Ce-modified catalysts, as demonstrated by H_2-TPR in Fig. 1(b) and (c). While coke accumulation is widely recognized as the primary deactivation mechanism in propane dehydrogenation, the sintering of Pt active sites also plays a significant role [3,23,70]. High temperatures encountered during dehydrogenation and regeneration cycles can induce severe sintering of Pt nanoparticles, often via Ostwald ripening. This results in the agglomeration of Pt particles into larger clusters, reducing the overall surface area and altering electronic properties essential for catalytic activity [6,71,72]. The resulting decrease in active site density leads to a substantial reduction in catalytic performance. HRTEM image of spent $PtGa/Al_2O_3$ catalyst (Figure S11) reveal a significant increase in metallic particle size compared to the fresh catalyst, confirming severe metal sintering at elevated reaction temperatures at prolong time. In contrast, the strong interactions between Pt, Ga, and Ce effectively inhibits Pt sintering because the robust Pt-O-Ce bond weakens the Pt-Pt bond and strengthens the Pt-O, suppressing Pt species sintering, as confirmed experimentally and theoretically [73,74]. Therefore, the presence of these strong interactions reduces Pt center sintering, prolonging the expected catalyst life, as shown in Fig. 4(c). To further explore the relationships between coke content and expected catalyst life, we exclude the effects of strong metal-support interactions and refit coke content against the expected catalyst life without Ce-modified catalysts (see Fig. 4(d)). Expectedly, a better linear correlation is achieved, suggesting that coke accumulation leads to poor catalyst stability.

Unlike intrinsic performance descriptors such as reducibility, and acid concentration, coke content accumulates progressively during reaction, should be viewed as an indicator of catalyst stability rather than an intrinsic feature of the fresh catalyst. Intrinsic structural factors–including Pt dispersity, Pt alloying, reducibility, and acid concentration–are central to defining initial catalytic properties, influencing activity, selectivity, and stability. Coke content, in contrast, is a dynamic characteristic arising from the interaction between these intrinsic features with the reaction environment under propane dehydrogenation conditions, serving as a downstream indicator of stability and durability rather than a primary factor governing initial catalytic performance. As coke accumulates over time, its development reflects the catalyst's inherent resistance to deactivation, especially through mechanisms involving Pt alloying and surface acid interactions. Thus, while coke content is indeed valuable as a stability metric, it is not a suitable pre-reaction descriptor of catalytic efficiency. Furthermore, we acknowledge that coke content is only one aspect of the catalyst's overall deactivation profiles. Additional factors such as Pt particle sintering and the potential leaching or loss of active components also significantly impact catalyst longevity and effectiveness. Overall, we continue to regard coke content as an essential indicator of catalyst stability, heavily influenced significantly by strong metal-support interactions, with its primary role in assessing catalyst stability rather than defining initial catalytic performance.

In delve into the mechanism for coke formation, DRIFTS measurements employing propylene as a probe molecule are conducted to examine propylene's interaction over different catalysts, as depicted in Fig. 4(e) and (f). Peaks around 1650 cm^{-1} correspond to the characteristic band of C═C bond stretching in propylene, while peaks around 1450 cm^{-1} represent the skeleton vibrations of aromatic rings [75]. The desorption peak of C═C bond stretching band over $PtGa/Al_2O_3$ catalyst remains unchanged after reaching 250 ℃, while the peak remains stable at 150 ℃ over $PtGa3Pr/Al_2O_3$ catalyst. These temperature-dependent desorption differences indicate the propylene desorption is more facile over promoted catalysts than over $PtGa/Al_2O_3$ catalyst. Moreover, the intensity of skeleton vibrations of aromatic ring increases with the gradual temperature increase, suggesting that the strong interaction between Pt and π-electrons of propylene leads to deep dehydrogenation of propylene to coke precursors [43]. Therefore, the easier desorption of propylene from Pt particles improves propylene selectivity and inhibits coke formation, resulting in superior catalytic performances.

4. Conclusions

In this work, we employed four promoters (La, Ce, Pr, and Nd) at varying loadings (1 wt%, 3 wt%, and 5 wt%) to enhance the performance of $PtGa/Al_2O_3$ catalyst in propane dehydrogenation. All resulting catalysts demonstrated significant improvements in conversion, selectivity, and stability when compared to the parent $PtGa/Al_2O_3$ catalyst. Importantly, we establish clear structure-activity relationships based on key performance descriptors. While reducibility proves to be an effective conversion descriptor, the impact of metal-support interactions should not be underestimated, particularly in the case of Ce-modified catalysts. On the other hand, total acid concentration emerges as an effective predictor of propylene selectivity, yet the surface chemical properties of Ga also play a crucial role in characterizing the trend. Unlike intrinsic descriptors for conversion and selectivity, coke content is valuable primarily as a post-reaction stability metric and therefore unsuitable as a pre-reaction indicator of catalyst stability. Nevertheless, it remains essential in accessing catalyst stability, with strong metal-support interactions heavily influencing its accumulation. Its role lies in gauging catalyst stability over time rather than defining initial catalytic

performance.

This exploration of diverse key performance descriptors in propane dehydrogenation provides a foundational approach to the rational design of catalysts and establishes a comprehensive framework for deriving catalytic descriptors applicable across industrial processes. It is believed that this work provides valuable insights into optimizing catalytic performance and advancing our understanding of the intricate relationships between catalyst composition, structure, and catalytic activity.

CRediT authorship contribution statement

Haokun Wang: Writing – review & editing, Methodology, Investigation, Formal analysis. **Xuelei Pan:** Methodology, Investigation, Formal analysis. **Yanjie Wang:** Methodology, Investigation. **Bryan Kit Yue Ng:** Methodology, Investigation. **S. C. Edman Tsang:** Writing – review & editing, Supervision.

Declaration of Competing Interest

The authors declare that they have no known competing financial interests or personal relationships that could have appeared to influence the work reported in this paper. Professor SCE Tsang reports financial support, administrative support, article publishing charges, and equipment, drugs, or supplies were provided by University of Oxford. If there are other authors, they declare that they have no known competing financial interests or personal relationships that could have appeared to influence the work reported in this paper

Acknowledgments

The authors gratefully acknowledge the financial support provided by the UK Engineering and Physical Sciences Research Council (EPSRC) under grant number EP/K040375/1. We extend our sincere thanks to Harwell XPS for facilitating the collection of XPS data under Contract No. PR16195. Additionally, we acknowledge the University of Surrey for their support in conducting Raman spectroscopy experiments.

Appendix A. Supporting information

Supplementary data associated with this article can be found in the online version at doi:10.1016/j.apcata.2024.120055.

Data Availability

Data will be made available on request.

References

[1] F. Feng, H. Zhang, S. Chu, Q. Zhang, C. Wang, G. Wang, F. Wang, L. Bing, D. Han, Recent progress on the traditional and emerging catalysts for propane dehydrogenation, J. Ind. Eng. Chem. 118 (2023) 1–18.
[2] K. Liang, X. Zeng, R. Ma, G. Zou, L. Dang, S. Li, A theoretical investigation of propane dehydrogenation on Pt and Ni-based alloys, J. Catal. 428 (2023) 115162.
[3] P. Wang, J. Yao, Q. Jiang, X. Gao, D. Lin, H. Yang, L. Wu, Y. Tang, L. Tan, Stabilizing the isolated Pt sites on PtGa/Al2O3 catalyst via silica coating layers for propane dehydrogenation at low temperature, Appl. Catal. B Environ. 300 (2022) 120731.
[4] J.H. Carter, T. Bere, J.R. Pitchers, D.G. Hewes, B.D. Vandegehuchte, C.J. Kiely, S. H. Taylor, G.J. Hutchings, Direct and oxidative dehydrogenation of propane: from catalyst design to industrial application, Green. Chem. 23 (2021) 9747–9799.
[5] A. Akah, J. Williams, M. Ghrami, An overview of light olefins production via steam enhanced catalytic cracking, Catal. Surv. Asia 23 (2019) 265–276.
[6] S. Chen, X. Chang, G. Sun, T. Zhang, Y. Xu, Y. Wang, C. Pei, J. Gong, Propane dehydrogenation: catalyst development, new chemistry, and emerging technologies, Chem. Soc. Rev. 50 (2021) 3315–3354.
[7] S. Kilmartin-Lynch, M. Saberian, J. Li, R. Roychand, G. Zhang, Preliminary evaluation of the feasibility of using polypropylene fibres from COVID-19 single-use face masks to improve the mechanical properties of concrete, J. Clean. Prod. 296 (2021) 126460.
[8] P.A. Payard, L. Rochlitz, K. Searles, L. Foppa, B. Leuthold, O.V. Safonova, A. Comas-Vives, C. Copéret, Dynamics and site isolation: keys to high propane dehydrogenation performance of silica-supported PtGa nanoparticles, JACS Au 1 (2021) 1445–1458.
[9] F. Yang, J. Zhang, Z. Shi, J. Chen, G. Wang, J. He, J. Zhao, R. Zhuo, R. Wang, Advanced design and development of catalysts in propane dehydrogenation, Nanoscale 14 (2022) 9963–9988.
[10] Z. Qu, Q. Sun, Advances in zeolite-supported metal catalysts for propane dehydrogenation, Inorg. Chem. Front. 9 (2022) 3095–3115.
[11] S. Chen, C. Pei, G. Sun, Z.-J. Zhao, J. Gong, Nanostructured catalysts toward efficient propane dehydrogenation, Acc. Mater. Res. 1 (2020) 30–40.
[12] M.-L. Yang, Y.-A. Zhu, X.-G. Zhou, Z.-J. Sui, D. Chen, First-principles calculations of propane dehydrogenation over PtSn catalysts, ACS Catal. 2 (2012) 1247–1258.
[13] B. Li, Z. Xu, F. Jing, S. Luo, W. Chu, Facile one-pot synthesized ordered mesoporous Mg-SBA-15 supported PtSn catalysts for propane dehydrogenation, Appl. Catal. A Gen. 533 (2017) 17–27.
[14] X.-Q. Gao, Z.-H. Yao, W.-C. Li, G.-M. Deng, L. He, R. Si, J.-G. Wang, A.-H. Lu, Calcium-modified PtSn/Al2O3 catalyst for propane dehydrogenation with high activity and stability, ChemCatChem 15 (2023) e202201691.
[15] X. Wu, Q. Zhang, L. Chen, Q. Liu, X. Zhang, Q. Zhang, L. Ma, C. Wang, Enhanced catalytic performance of PtSn catalysts for propane dehydrogenation by a Zn-modified Mg(Al)O support, Fuel Process. Technol. 198 (2020) 106222.
[16] M. Naseri, F. Tahriri Zangeneh, A. Taeb, The effect of Ce, Zn and Co on Pt-based catalysts in propane dehydrogenation, React. Kinet., Mech. Catal. 126 (2019) 477–495.
[17] Y. Qiu, X. Li, Y. Zhang, C. Xie, S. Zhou, R. Wang, S.-Z. Luo, F. Jing, W. Chu, Various metals (Ce, In, La, and Fe) promoted Pt/Sn-SBA-15 as highly stable catalysts for propane dehydrogenation, Ind. Eng. Chem. Res. 58 (2019) 10804–10818.
[18] G. Wang, K. Lu, C. Yin, F. Meng, Q. Zhang, X. Yan, L. Bing, F. Wang, D. Han, One-step fabrication of PtSn/γ-Al2O3 catalysts with La post-modification for propane dehydrogenation, Catalysts 10 (2020) 1042.
[19] B.K. Vu, M.B. Song, I.Y. Ahn, Y.-W. Suh, D.J. Suh, W.-I.L. Kim, H.-L. Koh, Y.G. Choi, E.W. Shin, Propane dehydrogenation over Pt–Sn/Rare-earth-doped Al2O3: influence of La, Ce, or Y on the formation and stability of Pt–Sn alloys, Catal. Today 164 (2011) 214–220.
[20] H. He, G.A. Canning, A. Nguyen, A. Dasgupta, R.J. Meyer, R.M. Rioux, M.J. Janik, Active-site isolation in intermetallics enables precise identification of elementary reaction kinetics during olefin hydrogenation, Nat. Catal. 6 (2023) 596–605.
[21] S.K. Kaiser, E. Fako, I. Surin, F. Krumeich, V.A. Kondratenko, E.V. Kondratenko, A. H. Clark, N. López, J. Pérez-Ramírez, Performance descriptors of nanostructured metal catalysts for acetylene hydrochlorination, Nat. Nanotechnol. 17 (2022) 606–612.
[22] T. Wang, F. Jiang, G. Liu, L. Zeng, Z.-j Zhao, J. Gong, Effects of Ga doping on Pt/CeO2-Al2O3 catalysts for propane dehydrogenation, AIChE J. 62 (2016) 4365–4376.
[23] Y. Nakaya, J. Hirayama, S. Yamazoe, K.-i Shimizu, S. Furukawa, Single-atom Pt in intermetallics as an ultrastable and selective catalyst for propane dehydrogenation, Nat. Commun. 11 (2020) 2838.
[24] J. Wu, G. Zhao, M. Song, H. Wang, Y. Wei, X. Chen, G. Wang, Z. Yan, Nanosheets-stacked Al2O3-flower anchoring Pt catalyst for intensified ethylene production from ethane dehydrogenation, Fuel 329 (2022) 125381.
[25] A.D. Prasetya, M. Rifai, Mujamilah, H. Miyamoto, X-ray diffraction (XRD) profile analysis of pure ECAP-annealing Nickel samples, J. Phys. Conf. Ser. 1436 (2020) 012113.
[26] R.-l Liu, H.-q Zhu, Z.-w Wu, Z.-f Qin, W.-b Fan, J.-g Wang, Aromatization of propane over Ga-modified ZSM-5 catalysts, J. Fuel Chem. Technol. 43 (2015) 961–969.
[27] G.L. Price, V. Kanazirev, Ga2O3/HZSM-5 propane aromatization catalysts: formation of active centers via solid-state reaction, J. Catal. 126 (1990) 267–278.
[28] E.L. Jablonski, A.A. Castro, O.A. Scelza, S.R. de Miguel, Effect of Ga addition to Pt/Al2O3 on the activity, selectivity and deactivation in the propane dehydrogenation, Appl. Catal. A: Gen. 183 (1999) 189–198.
[29] P. de La Bretèque, Gallium Bulletin Bibliographique, La Société, France S.A. Maraseille, 1974.
[30] M. Filez, E.A. Redekop, V.V. Galvita, H. Poelman, M. Meledina, S. Turner, G. Van Tendeloo, A.T. Bell, G.B. Marin, The role of hydrogen during Pt–Ga nanocatalyst formation, Phys. Chem. Chem. Phys. 18 (2016) 3234–3243.
[31] E.A. Redekop, V.V. Galvita, H. Poelman, V. Bliznuk, C. Detavernier, G.B. Marin, Delivering a modifying element to metal nanoparticles via support: Pt–Ga alloying during the reduction of Pt/Mg(Al,Ga)Ox catalysts and its effects on propane dehydrogenation, ACS Catal. 4 (2014) 1812–1824.
[32] T. Zhang, C. Pei, G. Sun, S. Chen, Z.-J. Zhao, S. Sun, Z. Lu, Y. Xu, J. Gong, Synergistic mechanism of platinum-GaOx catalysts for propane dehydrogenation, Angew. Chem. Int. Ed. 61 (2022) e202201453.
[33] H. Wang, T. Yoskamtorn, J. Zheng, P.-L. Ho, B. Ng, S.C.E. Tsang, Ce-promoted PtSn-based catalyst for hydrocracking of polyolefin plastic waste into high yield of gasoline-range products, ACS Catal. 13 (2023) 15886–15898.
[34] V. Pitchon, J.F. Zins, L. Hilaire, G. Maire, Influence of platinum on the reducibility of rare earth oxides supported on alumina, React. Kinet. Catal. Lett. 59 (1996) 203–209.
[35] C. Yu, Q. Ge, H. Xu, W. Li, Effects of Ce addition on the Pt-Sn/γ-Al2O3 catalyst for propane dehydrogenation to propylene, Appl. Catal. A: Gen. 315 (2006) 58–67.
[36] V. Zholobenko, C. Freitas, M. Jendrlin, P. Bazin, A. Travert, F. Thibault-Starzyk, Probing the acid sites of zeolites with pyridine: quantitative AGIR measurements of the molar absorption coefficients, J. Catal. 385 (2020) 52–60.

[37] Y. Sugi, Y. Kubota, K. Komura, N. Sugiyama, M. Hayashi, J.H. Kim, G. Seo, Shape-selective alkylation and related reactions of mononuclear aromatic hydrocarbons over H-ZSM-5 zeolites modified with lanthanum and cerium oxides, Appl. Catal. A Gen. 299 (2006) 157–166.
[38] Y. Yoshimura, N. Kijima, T. Hayakawa, K. Murata, K. Suzuki, F. Mizukami, K. Matano, T. Konishi, T. Oikawa, M. Saito, T. Shiojima, K. Shiozawa, K. Wakui, G. Sawada, K. Sato, S. Matsuo, N. Yamaoka, Catalytic cracking of Naphtha to light olefins, Catal. Surv. Jpn. 4 (2001) 157–167.
[39] K. Wakui, K.-i Satoh, G. Sawada, K. Shiozawa, K.-i Matano, K. Suzuki, T. Hayakawa, K. Murata, Y. Yoshimura, F. Mizukami, Catalytic cracking of n-butane over rare earth-loaded HZSM-5 catalysts, J. Jpn. Pet. Inst. 42 (1999) 307–314.
[40] M. Xue, Y. Zhou, Y. Zhang, X. Liu, Y. Duan, X. Sheng, Effect of cerium addition on catalytic performance of PtSnNa/ZSM-5 catalyst for propane dehydrogenation, J. Nat. Gas. Chem. 21 (2012) 324–331.
[41] R. Barth, R. Pitchai, R.L. Anderson, X.E. Verykios, Thermal desorption-infrared study of carbon monoxide adsorption by alumina-supported platinum, J. Catal. 116 (1989) 61–70.
[42] G. Blyholder, Molecular orbital view of chemisorbed carbon monoxide, J. Phys. Chem. 68 (1964) 2772–2777.
[43] Z. Lian, C. Si, F. Jan, S. Zhi, B. Li, Coke deposition on Pt-based catalysts in propane direct dehydrogenation: kinetics, suppression, and elimination, ACS Catal. 11 (2021) 9279–9292.
[44] Y. Zhang, M. Aly, Effect of CO2 on activity and coke formation over gallium-based catalysts for propane dehydrogenation, Appl. Catal. A Gen. 643 (2022) 118795.
[45] C. Sun, J. Luo, M. Cao, P. Zheng, G. Li, J. Bu, Z. Cao, S. Chen, X. Xie, A comparative study on different regeneration processes of Pt-Sn/γ-Al2O3 catalysts for propane dehydrogenation, J. Energy Chem. 27 (2018) 311–318.
[46] R. Alcala, D.P. Dean, I. Chavan, C.-W. Chang, B. Burnside, H.N. Pham, E. Peterson, J.T. Miller, A.K. Datye, Strategies for regeneration of Pt-alloy catalysts supported on silica for propane dehydrogenation, Appl. Catal. A Gen. 658 (2023) 119157.
[47] L. Ni, R. Khare, R. Bermejo-Deval, R. Zhao, L. Tao, Y. Liu, J.A. Lercher, Highly active and selective sites for propane dehydrogenation in zeolite Ga-BEA, J. Am. Chem. Soc. 144 (2022) 12347–12356.
[48] V.J. Cybulskis, S.U. Pradhan, J.J. Lovón-Quintana, A.S. Hock, B. Hu, G. Zhang, W. N. Delgass, F.H. Ribeiro, J.T. Miller, The nature of the isolated gallium active center for propane dehydrogenation on Ga/SiO2, Catal. Lett. 147 (2017) 1252–1262.
[49] A. Penkova, L.F. Bobadilla, F. Romero-Sarria, M.A. Centeno, J.A. Odriozola, Pyridine adsorption on NiSn/MgO–Al2O3: an FTIR spectroscopic study of surface acidity, Appl. Surf. Sci. 317 (2014) 241–251.
[50] L. Deng, J. Wang, Z. Wu, C. Liu, L. Qing, X. Liu, J. Xu, Z. Zhou, M. Xu, Effects of second metals (M = Fe, Cu, Ga, In, Sn) on the geometric and electronic properties of platinum for the direct dehydrogenation of propane, J. Alloy. Compd. 909 (2022) 164820.
[51] Y. Zhang, Y. Zhou, H. Liu, Y. Wang, Y. Xu, P. Wu, Effect of La addition on catalytic performance of PtSnNa/ZSM-5 catalyst for propane dehydrogenation, Appl. Catal. A Gen. 333 (2007) 202–210.
[52] E. Brack, M. Plodinec, M.-G. Willinger, C. Copéret, Implications of Ga promotion and metal–oxide interface from tailored PtGa propane dehydrogenation catalysts supported on carbon, Chem. Sci. 14 (2023) 12739–12746.
[53] G. Mitran, A. Urda, N. Tanchoux, F. Fajula, I.-C. Marcu, Propane oxidative dehydrogenation over Ln–Mg–Al–O catalysts (Ln = Ce, Sm, Dy, Yb), Catal. Lett. 131 (2009) 250–257.
[54] Z. Wang, Y. Chen, S. Mao, K. Wu, K. Zhang, Q. Li, Y. Wang, Chemical insight into the structure and formation of coke on PtSn alloy during propane dehydrogenation, Adv. Sustain. Syst. 4 (2020) 2000092.
[55] M. Kashif, M. Yuan, M. Abduallah, Y. Su, Fully selective catalytic oxidation of NO to NO2 over most active Ga-PCH catalyst, J. Environ. Chem. Eng. 8 (2020) 103524.
[56] S.E. Collins, M.A. Baltanás, J.L. Garcia Fierro, A.L. Bonivardi, Gallium–hydrogen bond formation on gallium and gallium–palladium silica-supported catalysts, J. Catal. 211 (2002) 252–264.
[57] X.-Q. Gao, W.-C. Li, B. Qiu, J. Sheng, F. Wu, A.-H. Lu, Promotion effect of sulfur impurity in alumina support on propane dehydrogenation, J. Energy Chem. 70 (2022) 332–339.
[58] Y. Zhang, Y. Zhou, M. Tang, X. Liu, Y. Duan, Effect of La calcination temperature on catalytic performance of PtSnNaLa/ZSM-5 catalyst for propane dehydrogenation, Chem. Eng. J. 181-182 (2012) 530–537.
[59] G. Wang, L. Zhou, S. Liu, N. Tang, C. Zhu, X. Zhu, C. Li, C. Yang, H. Shan, Highly active and stable Y2O3 promoted TiO2-ZrO2 catalyst for propane dehydrogenation, Chem. Eng. J. 477 (2023) 147047.
[60] S.T. Korhonen, S.M.K. Airaksinen, M.A. Bañares, A.O.I. Krause, Isobutane dehydrogenation on zirconia-, alumina-, and zirconia/alumina-supported chromia catalysts, Appl. Catal. A: Gen. 333 (2007) 30–41.
[61] Y.T. Chua, P.C. Stair, An ultraviolet Raman spectroscopic study of coke formation in methanol to hydrocarbons conversion over zeolite H-MFI, J. Catal. 213 (2003) 39–46.
[62] J. McGregor, Z. Huang, E.P.J. Parrott, J.A. Zeitler, K.L. Nguyen, J.M. Rawson, A. Carley, T.W. Hansen, J.-P. Tessonnier, D.S. Su, D. Teschner, E.M. Vass, A. Knop-Gericke, R. Schlögl, L.F. Gladden, Active coke: carbonaceous materials as catalysts for alkane dehydrogenation, J. Catal. 269 (2010) 329–339.
[63] A. Sadezky, H. Muckenhuber, H. Grothe, R. Niessner, U. Pöschl, Raman microspectroscopy of soot and related carbonaceous materials: spectral analysis and structural information, Carbon 43 (2005) 1731–1742.
[64] J. Liu, Z. Zhao, C. Xu, A. Duan, G. Jiang, J. Gao, W. Lin, I.E. Wachs, In-situ UV-Raman study on soot combustion over TiO2 or ZrO2-supported vanadium oxide catalysts, Sci. China Ser. B: Chem. 51 (2008) 551–561.
[65] J.J.H.B. Sattler, A.M. Beale, B.M. Weckhuysen, Operando Raman spectroscopy study on the deactivation of Pt/Al2O3 and Pt–Sn/Al2O3 propane dehydrogenation catalysts, Phys. Chem. Chem. Phys. 15 (2013) 12095–12103.
[66] Z. Han, S. Li, F. Jiang, T. Wang, X. Ma, J. Gong, Propane dehydrogenation over Pt–Cu bimetallic catalysts: the nature of coke deposition and the role of copper, Nanoscale 6 (2014) 10000–10008.
[67] M.S. Dresselhaus, G. Dresselhaus, A. Jorio, A.G. Souza Filho, R. Saito, Raman spectroscopy on isolated single wall carbon nanotubes, Carbon 40 (2002) 2043–2061.
[68] M. Dumont, G. Chollon, M.A. Dourges, R. Pailler, X. Bourrat, R. Naslain, J. L. Bruneel, M. Couzi, Chemical, microstructural and thermal analyses of a naphthalene-derived mesophase pitch, Carbon 40 (2002) 1475–1486.
[69] H.-Z. Wang, L.-L. Sun, Z.-J. Sui, Y.-A. Zhu, G.-H. Ye, D. Chen, X.-G. Zhou, W.-K. Yuan, Coke formation on Pt–Sn/Al2O3 catalyst for propane dehydrogenation, Ind. Eng. Chem. Res. 57 (2018) 8647–8654.
[70] N.V. Srinath, A. Longo, H. Poelman, R.K. Ramachandran, J.-Y. Feng, J. Dendooven, M.-F. Reyniers, V.V. Galvita, In situ XAS/SAXS study of Al2O3-coated PtGa catalysts for propane dehydrogenation, ACS Catal. 11 (2021) 11320–11335.
[71] L. Wang, L. Wang, X. Meng, F.-S. Xiao, New Strategies for the preparation of sinter-resistant metal-nanoparticle-based catalysts, Adv. Mater. 31 (2019) 1901905.
[72] J. Zhu, M.-L. Yang, Y. Yu, Y.-A. Zhu, Z.-J. Sui, X.-G. Zhou, A. Holmen, D. Chen, Size-dependent reaction mechanism and kinetics for propane dehydrogenation over Pt catalysts, ACS Catal. 5 (2015) 6310–6319.
[73] Q. Ning, H. Zhang, Y. He, Z. Chen, S. Liu, J. Ren, Suppression of platinum sintering on Pt–M/ZSM-22 (M = Ce, La, and Re) catalyst for n-dodecane isomerization, N. J. Chem. 43 (2019) 13967–13978.
[74] F. Ahmed, M.K. Alam, R. Muira, A. Suzuki, H. Tsuboi, N. Hatakeyama, A. Endou, H. Takaba, M. Kubo, A. Miyamoto, Adsorption and dissociation of molecular hydrogen on Pt/CeO2 catalyst in the hydrogen spillover process: a quantum chemical molecular dynamics study, Appl. Surf. Sci. 256 (2010) 7643–7652.
[75] W. Zhang, H. Wang, J. Jiang, Z. Sui, Y. Zhu, D. Chen, X. Zhou, Size dependence of Pt catalysts for propane dehydrogenation: from atomically dispersed to nanoparticles, ACS Catal. 10 (2020) 12932–12942.